

# Rep3Net: An Approach Exploiting Multimodal Representation for Molecular Bioactivity Prediction

Sabrina Islam, Md. Atiqur Rahman, Md. Bakhtiar Hasan, and \*Md. Hasanul Kabir

Computer Science and Engineering, Islamic University of Technology, Bangladesh

\*hasanul@iut-dhaka.edu

## Abstract

In early stage drug discovery, bioactivity prediction of molecules against target proteins plays a crucial role. Traditional QSAR models that utilize molecular descriptor based data often struggle to predict bioactivity of molecules effectively due to its limitation in capturing structural and contextual information embedded within each compound. To address this challenge, we propose Rep3Net, a unified deep learning architecture that not only incorporates descriptor data but also includes spatial and relational information through graph-based representation of compounds and contextual information through ChemBERTa generated embeddings from SMILES strings. Our model employing multimodal concatenated features produce reliable bioactivity prediction on Poly [ADP-ribose] polymerase 1 (PARP-1) dataset. PARP-1 is a crucial agent in DNA damage repair and has become a significant therapeutic target in malignancies that depend on it for survival and growth. A comprehensive analysis and comparison with conventional standalone models including GCN, GAT, XGBoost, etc. demonstrates that our architecture achieves the highest predictive performance. In computational screening of compounds in drug discovery, our architecture provides a scalable framework for bioactivity prediction.

## Keywords

Molecular Representation, Poly [ADP-ribose] polymerase 1 (PARP-1), Molecular bioactivity prediction, Drug Discovery.

## Introduction

In biochemistry, inhibitor compounds are responsible for limiting or stopping a chemical or biological process. Additionally, these substances can also slow the growth of proteins that help in the progression of diseases and cancers. To identify potential drugs, inhibitory compounds are therefore identified against target proteins. Traditionally, these compounds are identified through clinical trials which are expensive, time consuming and labor intensive. To overcome this issue, computational methods are now adopted to perform the initial screening of compounds from the huge chemical library. Quantitative Structure-Activity Relationship (QSAR) is a computational strategy that predicts a chemical compound's bioactivity with a target protein through machine learning and deep learning methods [1].

Poly [ADP-ribose] polymerase 1 (PARP-1) is an enzyme that plays a significant role in repairing damaged DNA of cancer cells through the base excision repair pathway [2]. DNA breaks are promptly bound by PARP1, which initiates its catalytic activity, leading to the attachment of long, branched, negatively charged poly(ADP-ribose) (PAR) polymer chains (PARylation) onto itself and other nearby proteins [3]. This enzyme activity supports the survival and growth of cancer cells by allowing cells to repair damaged DNA. In addition to relaxing chromatin at the site of damage, PARylation acts as a molecular scaffold that attracts PAR-binding proteins for subsequent DNA repair processes [4]. Consequently, inhibition of PARP-1 has now become an effective therapeutic approach, especially for homologous recombination (HR) deficient BRCA1

or BRCA2 mutations [5, 6]. Alongside the ongoing clinical trials PARP-1 inhibitors which is an expensive and lengthy process [7, 8], various computational methods are being applied. Effective prediction through computational approach can significantly lessen reliance on manual labor in early stage research and improve the overall efficiency of the drug development process [9] against PARP-1. In most computational approaches, the inhibitory compound is identified through the prediction of IC50 values. IC50 value is the concentration needed to inhibit a biological function by 50% [10] and it is a great measure of a compound’s inhibitory strength toward a target protein. Diverse data can be achieved through a substances canonical smile string that can be processed to and feed to a computational model to predict IC50 values.

In this study, our main contributions are:

- Combination of three different input feature types from a single compound: molecular descriptors, graph-based spatial information, and embedded information from canonical smile to produce a feature vector rich in compounds structural and contextual information.
- IC50 value prediction of chemical compounds against PARP1 which has proved to be a critical therapeutic target in various cancers.
- A comprehensive evaluation, analysis on a diverse set of models and comparison with our architecture providing insightful information for future inhibitor prediction studies.

## Background Study

With the growing need for quick and affordable identification of therapeutically relevant molecules, the area of computational drug design has advanced rapidly. There are several different computational paradigms that can be identified mainly by the way molecular structures are modeled. The molecular representations include descriptor-based approaches, graph-based representations, and SMILES-driven sequence models. Open-source frameworks such as RDKit have become standard tools to calculate molecular descriptor values due to their extensive feature libraries, reproducibility, and ease of integration into machine learning pipelines. When trained on descriptor-level features, traditional machine learning algorithms like Random Forest, XGBoost, Support Vector Machines, and K-Nearest Neighbors have shown strong predictive performance. However, despite these achievements, descriptor-based QSAR models have intrinsic drawbacks. Their capacity to capture more complex chemical interactions and structural subtleties is limited by their dependence on predetermined, human-engineered features. Incomplete or noisy data, which are common in real-world drug research, may cause these models to perform badly. Consequently, the field has shifted increasingly toward contemporary data-driven approaches like graph neural networks.

SMILES strings are well-suited for natural language processing (NLP) methods because they capture sequential and contextual chemical information, in contrast to graph-based representations that focus on structural connectedness. Recent developments in deep learning have demonstrated a great ability to extract long-range and semantic connections from SMILES sequences, especially Transformer-based language models. These models use self-attention techniques to learn tiny interaction patterns that greatly improve molecular property and bioactivity prediction by treating molecular strings as chemical language. Consequently, in contemporary QSAR and drug discovery pipelines, SMILES-based transformer models have become a potent addition to graph neural networks.

Although descriptor-based models, graph neural networks, and SMILES-based transformer architectures have each shown effectiveness in inhibitor prediction tasks such as in studies targeting BACE-1 inhibitors and other enzymatic systems, these approaches have mostly been investigated separately. To the best of our knowledge, no previous work has created a cohesive modeling framework by concurrently integrating these three molecular views.

Recent research emphasizes the therapeutic significance of PARP-1 (Poly(ADP-ribose) polymerase-1) inhibition, especially in malignancies with BRCA mutations, where survival depends on PARP-mediated DNA repair pathways due to abnormalities in homologous recombination repair [11]. As a result, PARP-1 has become a promising therapeutic target, and PARP inhibitors are well known for being effective alongside chemotherapy and radiations in a variety of cancers [12–14]. Although several computational studies have attempted to predict PARP-1 inhibitors, they have mostly relied on conventional descriptor-based QSAR models [15–17], that do not incorporate more comprehensive multimodal chemical representations. There

is currently a large performance and methodological gap in the field because no work has used a unified deep learning pipeline including descriptors, graph representations, and SMILES embeddings for PARP-1 inhibitor prediction.

## Methods

### Dataset

ChEMBL [18] is a manually curated, high-quality, large-scale, and open resource of over two billion bioactive molecules with drug-like properties. We obtained bioactivity information solely for Human PARP 1 (ChEMBL3105) encompassing 4,802 compounds, from the database.

### Preprocessing

The collected dataset consisted of molecular compounds with IC50 as the activity type. To ensure consistency and reliability, the dataset was systematically filtered based on several criteria. Only entries with a standard relation of '=' were retained, excluding values reported as greater-than, less-than, or approximate measurements. The standard unit was restricted to nanomolar (nM) to maintain uniformity in activity scale, and compounds lacking canonical SMILES were removed. Multiple entries representing the same compound were identified and instead of discarding duplicates, we aggregated them using the median IC50 value to minimize the effect of experimental variation. These filtering process yielded 3,356 unique samples, which were then used to train and evaluate the baseline methods with Rep3Net.

Training a regressor with IC50 values generate a high loss during initial phases due to the huge difference between the minimum and maximum IC50 values of the chemical compounds. Thus, we have chosen to convert IC50 to pIC50 values using the Eq. 1. Additionally, for a more stable training environment we have standardized pIC50 values using StandardScaler [19].

$$pIC50 = -\log_{10}IC50 \tag{1}$$

### Input Representation

In our proposed architecture, each compound was represented using three complementary input modalities:

- Molecular descriptors,
- Embeddings from MLM, and,
- Graph based representation.

### Molecular Descriptors

Molecular descriptors provide a numerical representation of the basic structural and chemical properties of compounds [20]. These numerical values are very important to represent chemical compounds in a way so that computing models can characterize, compare and analyze different chemical compounds. These descriptors serve as feature inputs for machine learning and deep learning models in drug discovery, property prediction and similarity search. We have used RDKit software to produce 217 molecular descriptors for each chemical compound. We investigated and found multiple redundant descriptors and decided to perform the following filtering steps so that we can retain the most informative and unique subset of descriptors, improving training efficiency and stability:

- Some descriptors exhibit extremely low variance; for example, certain descriptors take nearly identical values across all chemical compounds. These descriptors having **lower variance than 0.01**, were removed.
- To address correlation among the available numerical features, for each pair of descriptors with a **correlation coefficient greater than 0.9**, one feature was discarded based on an upper-triangular filtering strategy.

- Finally, feature values were standardized using the StandardScaler method.

These cleansing steps resulted in a final number of 134 molecular descriptors for each compound.

## Embeddings from MLM

Numerical representation by molecular descriptor shows attribute of structural and chemical properties, However, the properties of a molecule may change based on the other molecules it interacts with. To tackle this issue, we have used embeddings generated by ChemBERTa, a Masked Language Model(MLM) [21] using only SMILES as input. These embeddings will provide rich information about chemical semantics, substructure patterns, and functional group interactions, learned by ChemBERTa during heavy self supervised pretraining on chemical language corpora. Each compound’s canonical SMILES notation was tokenized and passed through the pretrained ChemBERTa model. After the forward pass, we extracted the output from the last hidden layer, bypassing the prediction head to obtain feature representations instead of model outputs.

## Graph Representation

Molecules can naturally be presented in graphs, where atoms can be nodes and bonds can be edges. To exploit the spatial and relational information of a molecule in a more faithful way, we have chosen graphical features of that molecule as our one of the input to our Rep3Net. To obtain graph based molecular representations, we used the DGL-LifeSci toolkit to convert SMILES strings into graph  $G = (V, E)$ , where node  $v \in V$  denotes atom and edge  $e \in E$  denotes bond [22]. Moreover, featurizers from the toolkit, gives a set of numerical values depending on the atoms and bonds presented in the SMILES string. These numerical values works as features that can be understood by Graphical Neural Networks (GNNs) and also can be static or dynamic depending on the type of featurizers. The GNN baselines we have employed most use Canonical featurizers where only AttentiveFP network has its own featurizer. The Canonical featurizer generates traditional feature vectors that serve as a comprehensive set of handcrafted descriptors that preserve chemically important information. On the contrary, AttentiveFP’s featurizer provide learned embeddings that captures interaction patterns that may not be explicitly encoded in handcrafted features.

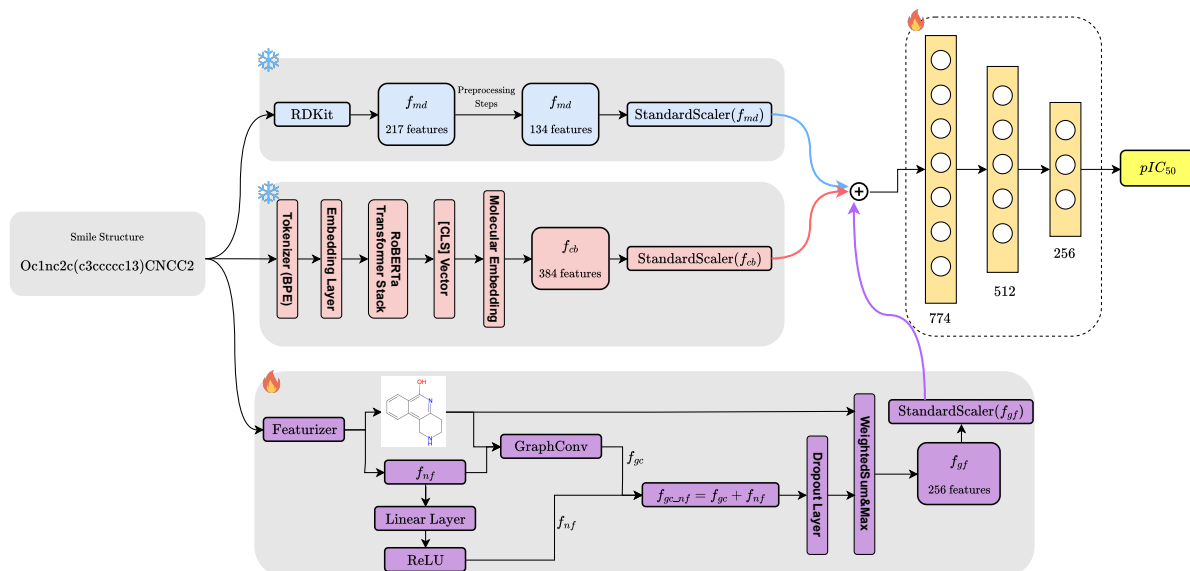


Figure 1: Proposed Architecture

## Proposed Architecture

We propose Rep3Net that integrates three complementary molecular input representations: molecular descriptors, ChemBERTa SMILES embeddings, and graph based features, into a unified predictive framework. The architecture is depicted in Figure 1 and demonstrated in algorithm 1.

Due to the absence of pretrained graph neural networks tailored for PARP-1 inhibitor data, the graph representations generated from DGL-LifeSci were processed through GNN module of Rep3Net to extract spatially informed feature vectors. Our GNN module follow the Eq. 2 to provide the graph based features. Initially, the featurizer extract the graph  $G_i$  and numerical vectors  $F_{l,i}$  using SMILES  $S_i$  of  $i^{th}$  molecule in our dataset.  $G_i$  represents the atoms and bonds in the  $S_i$  as nodes and edges where  $F_{l,i}$  depicts the attribute of each atom and bonds. Then, we have employed a graph convolutional layer with a skip connection, that produce features  $F_{gc,i}$ . After that, we pass the features through a Dropout layer and  $\varphi$ , a weighted sum and max pooling layer specifically build for GNNs. This layer produced  $f_{g,i}$ , a concatenated features from two compact representations of  $F_{gc,i}$ . One representation has added feature values depending on the importance of a node and another has only max feature values. Finally, we produce  $\hat{f}_{g,i}$  by standardizing  $f_{g,i}$  using Standard Scaler approach.

$$\begin{aligned} G_i, F_{l,i} &= \text{Featurizer}(S_i), \\ f_{gc,i} &= \text{GraphConv}(G_i, F_{l,i}), \\ f_{l,i} &= \text{ReLU}(\text{Linear}(F_{l,i})), \\ F_{gc,i} &= f_{gc,i} + f_{l,i}, \\ f_{g,i} &= \varphi(\text{Dropout}(F_{gc,i}), G_i), \\ \hat{f}_{g,i} &= \delta(f_{g,i}) \end{aligned} \tag{2}$$

While the above procedure is going on to generate graph based features  $\hat{f}_{g,i}$ , other path ways of Rep3Net parallely produce fixed molecular descriptors and contextual enriched embeddings from ChemBERTa, depicted in Eq. 3. After, the generation of all the three features, we concatenate ( $\oplus$ ) them and pass it through Rep3Net’s Regressor as shown in Eq. 4. The Regressor module consists of three fully connected layers, each followed by Batch Normalization, ReLU activation and Dropout for stable and efficient learning.

$$\begin{aligned} \hat{f}_{md,i} &= \delta(\text{RDKit}(S_i)), \\ \hat{f}_{cb,i} &= \delta(\text{ChemBERTa}(S_i)) \end{aligned} \tag{3}$$

$$Y_i = \text{Regressor}(\hat{f}_{md,i} \oplus \hat{f}_{cb,i} \oplus \hat{f}_{g,i}) \tag{4}$$

---

**Algorithm 1:** Fusion-based regression model for IC50 prediction

---

**Function** PARP\_Fusion\_Regression( $bg, cb, md$ ):

- Input:**  $bg$  – batched molecular graph
- Input:**  $cb$  – ChemBERTa embedding vector
- Input:**  $md$  – molecular descriptor vector
- Output:**  $\hat{y}$  – predicted IC50 value

```
1  node_feats ← GNN(bg, bg.node_features)
2  graph_feats ← READOUT(bg, node_feats)
3  // Normalize inputs
4  md ← (md – mean(md))/(std(md) + ε)
5  cb ← (cb – mean(cb))/(std(cb) + ε)
6  graph_feats ← (graph_feats – mean(graph_feats))/(std(graph_feats) + ε)
7  // Feature fusion
8  x ← Concatenate(graph_feats, cb, md)
9  // Fully-connected regression network
10 x ← Dropout(ReLU(BatchNorm(FC1(x))))
11 x ← Dropout(ReLU(BatchNorm(FC2(x))))
12  $\hat{y}$  ← FC3(x)
13 return  $\hat{y}$ 
```

---

## Evaluation Metrics

To comprehensively assess the performance of our regression models, we employed six widely used evaluation metrics: Mean Squared Error (MSE), Root Mean Squared Error (RMSE), Mean Absolute Error (MAE), Coefficient of Determination ( $R^2$ ), Pearson Correlation Coefficient, and Spearman Rank Correlation Coefficient. These metrics collectively evaluate prediction accuracy, error magnitude, and the strength of association between predicted and actual values.

### Mean Squared Error (MSE)

MSE quantifies the average squared difference between the predicted values  $\hat{y}_i$  and the actual target values  $y_i$ . Because the errors are squared, larger deviations are penalized more heavily.

$$\text{MSE} = \frac{1}{n} \sum_{i=1}^n (y_i - \hat{y}_i)^2$$

### Root Mean Squared Error (RMSE)

RMSE is the square root of MSE, providing an interpretable measure in the same units as the target variable. It remains sensitive to large prediction errors.

$$\text{RMSE} = \sqrt{\frac{1}{n} \sum_{i=1}^n (y_i - \hat{y}_i)^2}$$

### Mean Absolute Error (MAE)

MAE calculates the average magnitude of prediction errors without considering direction. Unlike MSE and RMSE, it treats all deviations equally, making it robust to outliers.

$$\text{MAE} = \frac{1}{n} \sum_{i=1}^n |y_i - \hat{y}_i|$$

## R-squared ( $R^2$ )

The  $R^2$  score represents the proportion of the total variance in the observed data that is explained by the model. It ranges from  $-\infty$  to 1, where higher values indicate better predictive performance.

$$R^2 = 1 - \frac{\sum_{i=1}^n (y_i - \hat{y}_i)^2}{\sum_{i=1}^n (y_i - \bar{y})^2}$$

where  $\bar{y}$  is the mean of the actual values.

## Pearson correlation

Pearson correlation evaluates the strength and direction of a linear relationship between actual and predicted values.

$$r = \frac{\sum_{i=1}^n (y_i - \bar{y})(\hat{y}_i - \bar{\hat{y}})}{\sqrt{\sum_{i=1}^n (y_i - \bar{y})^2} \sqrt{\sum_{i=1}^n (\hat{y}_i - \bar{\hat{y}})^2}}$$

## Spearman correlation

Spearman correlation measures the strength and direction of a monotonic (not necessarily linear) relationship. It is computed on the ranked values of the variables, making it suitable for data not following a normal distribution.

$$\rho = 1 - \frac{6 \sum_{i=1}^n d_i^2}{n(n^2 - 1)}$$

where  $d_i$  is the difference between the ranks of  $y_i$  and  $\hat{y}_i$ .

# Results and discussion

In this work, we aim to predict the pIC50 values of chemical compounds directly from their structural information. To capture this structure–activity relationship, we experiment with three different representations of the same molecule, traditional molecular descriptors, learned embeddings from ChemBERTa, and graph-based representations. Although the primary task is regression, the predictions can be easily adapted to a classification setting, allowing us to determine whether a compound is likely to function as a PARP inhibitor based on its predicted pIC50. In essence, the goal is to assess compound activity using structural cues alone. The following subsections present the results obtained from comparing our architecture with state-of-the-art classical nonlinear and graph based models, and include an ablation study that highlights the contributions of our design along with an analysis of its computational efficiency.

## Performance of Classical Architectures

In classical QSAR modeling, the standard practice is to rely solely on molecular descriptors as input features. However, as shown in Table 1, classical methods perform poorly on our dataset yielding a negative  $R^2$  score, indicating that predicting the mean pIC50 for all molecules would outperform these methods. We identify three key factors that likely hinder these methods from learning the underlying structure–activity relationship in this task:

- **Data Sparsity:** The molecular descriptors exhibit very limited variance, with most values clustered closely together. This lack of diversity makes it difficult for classical algorithms to detect meaningful or discriminative patterns.
- **Activity Cliffs:** Bioactivity prediction is highly susceptible to activity cliffs, where small structural changes can lead to large shifts in pIC50. Capturing these abrupt changes is especially challenging for classical nonlinear models when the descriptors show little variation.
- **Small Training Set:** With only 2,516 samples in the training set, the limited data amplifies the effects of sparsity and activity cliffs constraining the ability of classical methods to learn stable and reliable structure–activity relationships.

Table 1: Performance of Standard Classical Architectures on PARP Inhibitors Regression Task

Model	MSE ↓	RMSE ↓	MAE ↓	$R^2$ ↑	Pearson ↑	Spearman ↑
RandomForest	$1.04 \pm 0.08$	$1.02 \pm 0.04$	$0.83 \pm 0.02$	$-0.05 \pm 0.03$	$0.02 \pm 0.05$	$0.02 \pm 0.06$
XGBoost	$1.00 \pm 0.10$	$1.00 \pm 0.05$	$0.81 \pm 0.02$	$-0.001 \pm 0.00$	$0.01 \pm 0.10$	$-0.00 \pm 0.12$
KNN	$1.16 \pm 0.04$	$1.08 \pm 0.02$	$0.88 \pm 0.02$	$-0.17 \pm 0.09$	$0.02 \pm 0.08$	$0.01 \pm 0.09$

## Performance of Baseline GNN methods

In Table 2, we can find our methods is the best among all the baseline GNN in all six evaluation metrics.

GAT [23] leverages attention mechanisms to learn weighted contributions of neighboring nodes when updating node representations. Only considering neighboring nodes may not be enough to capture the complex structure-activity relationship with only few samples to train on. 34.4% more  $R^2$  means, our methods is more capable to capture the variations of pIC50 values than GAT.

Weave [24] focuses primarily on local chemical environments through shallow message passing approach, which limits its ability to capture broader structural patterns. On the contrary, our architecture integrates multiple complementary views of each molecule, such as, global molecular descriptors, contextual ChemBERTa embeddings, and learnable spatial representation of a molecule using graph, providing a richer and complete understanding of molecular structure. This fusion of diverse features enables our architecture to learn subtle structure-activity signals that Weave’s strictly local message passing framework cannot capture. The advantage is clearly reflected in the results where our model improves Spearman correlation by approximately 17.54% and reduces MSE by roughly 20.2% compared to Weave.

MPNN [25] updates node representations by iteratively aggregating messages from neighboring nodes over the molecular graph. This approach heavily depends on graph topology and the node or edge features provided, which can limit its ability to integrate broader chemical context. However, our approach not only using graph representation but also depending on molecular descriptor and learned embeddings of chemBERTa, exploit the broader chemical context and increase upto 20% in pearson correlation metric than standard MPNN approach.

AttentiveFP [26] extends graph attention by applying a hierarchical attention mechanism at both the atom and molecule levels. This allows the model to focus on important substructures while learning molecular embeddings. However, the attention mechanism under performs when there is not enough graphical structures to generalize properly, hence almost 15% less spearman correlation with the actual pIC50 values of the chemical compounds compared to our approach, that works well even in low data scenario exploiting diverse features.

Table 2: Performance Comparison with GNN baselines

Model	MSE ↓	RMSE ↓	MAE ↓	$R^2$ ↑	Pearson ↑	Spearman ↑
GAT	$0.99 \pm 0.11$	$1.00 \pm 0.06$	$0.78 \pm 0.02$	$0.32 \pm 0.06$	$0.57 \pm 0.05$	$0.59 \pm 0.03$
Weave	$1.04 \pm 0.14$	$1.02 \pm 0.07$	$0.79 \pm 0.02$	$0.29 \pm 0.06$	$0.54 \pm 0.05$	$0.57 \pm 0.03$
MPNN	$1.03 \pm 0.14$	$1.02 \pm 0.07$	$0.78 \pm 0.03$	$0.30 \pm 0.05$	$0.55 \pm 0.05$	$0.55 \pm 0.03$
AttentiveFP	$1.04 \pm 0.14$	$1.02 \pm 0.07$	$0.80 \pm 0.03$	$0.29 \pm 0.05$	$0.54 \pm 0.05$	$0.57 \pm 0.04$
<b>Ours</b>	<b><math>0.83 \pm 0.06</math></b>	<b><math>0.91 \pm 0.03</math></b>	<b><math>0.69 \pm 0.02</math></b>	<b><math>0.43 \pm 0.01</math></b>	<b><math>0.66 \pm 0.01</math></b>	<b><math>0.67 \pm 0.01</math></b>

## Computational Cost Analysis

Table 3 compares the computational efficiency of several graph based models by considering their amount of trainable parameters and inference time per sample as metrics. The results show that inference latency depends not only on model size but also on architectural design.

Weave has highest speed during inference taking only 0.66 ms per sample where having triple number of parameters than AttentiveFP, the smallest model among all the baselines. Moreover, GAT also takes lower time in inference than most methods. Although Weave has half the number of parameters than GAT, the difference between their inference speed is only 0.11 ms. We conclude that the forward mechanisms of

both Weave and GAT, which involve computationally inexpensive operations, contribute to their superior inference performance in terms of time per sample.

Additionally, in spite of having the fewest parameters (0.01M), AttentiveFP requires 1.8 ms per sample. This is because AttentiveFP relies on multiple stacked attention layers and iterative readout operations, which introduce computational overhead through sequential attention steps that are not easily parallelizable. Thus, even with a small parameter count, the model incurs additional latency due to its deeper and more complex operations.

Moreover, MPNN has 0.35M parameters and shows the highest inference time (3.2 ms), where Rep3Net having the largest parameter count of 0.55M, takes only 0.7 ms to process a sample during inference. This reflects the computational cost of multiple message-passing steps and complex neighborhood aggregation routines of MPNN, which involve repeated graph traversals. We contribute the following three attributes of Rep3Net for its efficiency during inference despite having the largest parameter count:

- It uses only a single graph convolution layer with a canonical featurizer, leveraging static structural features of the chemical compound.
- In parallel, it generates ChemBERTa and RDKit-based embeddings without relying on iterative readout mechanisms.
- The absence of deep attention stacks or repeated message-passing steps eliminates much of the overhead seen in AttentiveFP and MPNN.

Overall, these findings demonstrate that the proposed model provides a strong trade-off between representational capacity and computational efficiency, outperforming more complex architectures in runtime while maintaining competitive expressiveness.

Table 3: Computational Cost Analysis

Model	Total Trainable Parameters ( $10^6$ )	Inference Time Per Sample (milliseconds)
GAT	0.06	0.77
Weave	<b>0.03</b>	0.66
MPNN	0.35	3.2
AttentiveFP	0.01	1.8
Ours	0.55	<b>0.7</b>

## Ablation Study

To assess the individual and combined contributions of the representations used in our model, we conducted an ablation study across seven configurations, as shown in Table 4. Using only molecular descriptors results in an MSE of 1.06 and a Spearman correlation of 0.58, while relying solely on ChemBERTa embeddings improves performance to an MSE of 0.94 and Spearman 0.63. The graph based representations alone performs even better, achieving an MSE of 0.90 and Spearman 0.66, highlighting the strong predictive value of structural graph information. Combining two representations—such as descriptors with ChemBERTa embeddings or ChemBERTa embeddings with the graph based representations, yields further gains, with MSE values ranging from 0.89 to 0.91 and Spearman correlations between 0.65 and 0.67. The complete model, which integrates all three representations, delivers the strongest performance, achieving an MSE of 0.84 and Spearman 0.68. These results demonstrate that molecular descriptors, contextual ChemBERTa embeddings, and graph based structural reasoning complement one another, and their synergy leads to the highest predictive accuracy.

## Statistical Significance

We employed 5-fold cross-validation to evaluate all classical methods, GNN baselines, and our proposed model. Each model was tested five times, and 95% confidence intervals were calculated for the evaluation

Table 4: Ablation Study

Molecular Descriptor	ChemBerta Representation	Graph Neural Network	MSE ↓	Spearman ↑
✓			1.06	0.58
	✓		0.94	0.63
		✓	0.90	0.66
✓	✓		0.91	0.65
	✓	✓	0.89	0.66
✓		✓	0.89	0.67
✓	✓	✓	<b>0.84</b>	<b>0.68</b>

metrics and shown in Table 2. Across all metrics, our model consistently exhibits the lowest or among the lowest deviations from the mean, with a reduction in deviation of up to 57% in MSE. This indicates that, in addition to accurately predicting pIC50 values, our approach provides more reliable and stable predictions compared to the baseline methods.

## Conclusion

We introduced a novel deep learning framework for molecular inhibitor prediction that integrates three widely used yet previously isolated molecular representation techniques. By combining these complementary representations into a unified feature vector, we are exploiting rich structural and chemical properties, contextual information and learnable spatial attribute of a molecule to predict its characteristic as an inhibitor. Our results highlight clear performance improvements over conventional approaches, establishing the value of multimodal feature learning in drug discovery tasks. Furthermore, we applied this framework to the prediction of PARP-1 inhibitors, an important class of compounds targeting DNA repair pathways in BRCA-mutated cancers, indicating its potential for accelerating early stage virtual drug screening and prioritizing candidate molecules for physical experimental validation. Future work will focus on expanding the model to larger chemical spaces, and exploring explainable AI approaches for enhancing the interpretability of Rep3Net.

## References

- (1) Cherkasov, A.; Muratov, E. N.; Fourches, D.; Varnek, A.; Baskin, I. I.; Cronin, M.; Dearden, J.; Gramatica, P.; Martin, Y. C.; Todeschini, R., et al. *Journal of medicinal chemistry* **2014**, *57*, 4977–5010.
- (2) Morales, J.; Li, L.; Fattah, F. J.; Dong, Y.; Bey, E. A.; Patel, M.; Gao, J.; Boothman, D. A. *Critical Reviews™ in Eukaryotic Gene Expression* **2014**, *24*.
- (3) Pascal, J. M.; Ellenberger, T. *DNA repair* **2015**, *32*, 10–16.
- (4) Teloni, F.; Altmeyer, M. *Nucleic acids research* **2015**, *44*, 993–1006.
- (5) Kanev, P.-B.; Atemin, A.; Stoyanov, S.; Aleksandrov, R. In *Seminars in oncology*, 2024; Vol. 51, pp 2–18.
- (6) Lord, C. J.; Ashworth, A. *Science* **2017**, *355*, 1152–1158.
- (7) Mateo, J.; Lord, C.; Serra, V.; Tutt, A.; Balmaña, J.; Castroviejo-Bermejo, M.; Cruz, C.; Oaknin, A.; Kaye, S.; De Bono, J. *Annals of Oncology* **2019**, *30*, 1437–1447.
- (8) LaFargue, C. J.; Dal Molin, G. Z.; Sood, A. K.; Coleman, R. L. *The Lancet Oncology* **2019**, *20*, e15–e28.
- (9) Vamathevan, J.; Clark, D.; Czodrowski, P.; Dunham, I.; Ferran, E.; Lee, G.; Li, B.; Madabhushi, A.; Shah, P.; Spitzer, M., et al. *Nature reviews Drug discovery* **2019**, *18*, 463–477.

- (10) Sebaugh, J. *Pharmaceutical statistics* **2011**, *10*, 128–134.
- (11) Weaver, A. N.; Yang, E. S. *Frontiers in oncology* **2013**, *3*, 290.
- (12) Calabrese, C. R.; Almassy, R.; Barton, S.; Batey, M. A.; Calvert, A. H.; Canan-Koch, S.; Durkacz, B. W.; Hostomsky, Z.; Kumpf, R. A.; Kyle, S., et al. *Journal of the National Cancer Institute* **2004**, *96*, 56–67.
- (13) Plummer, R.; Jones, C.; Middleton, M.; Wilson, R.; Evans, J.; Olsen, A.; Curtin, N.; Boddy, A.; McHugh, P.; Newell, D., et al. *Clinical cancer research* **2008**, *14*, 7917–7923.
- (14) Khan, O.; Gore, M.; Lorigan, P.; Stone, J.; Greystoke, A.; Burke, W.; Carmichael, J.; Watson, A. J.; McGown, G.; Thorncroft, M., et al. *British journal of cancer* **2011**, *104*, 750–755.
- (15) Shahab, M.; Waqas, M.; Fahira, A.; Sharma, B. P.; Zhang, H.; Zheng, G.; Huang, Z. *Molecular Diversity* **2025**, 1–21.
- (16) Gomatam, A.; Hirlekar, B. U.; Singh, K. D.; Murty, U. S.; Dixit, V. A. *Molecular Diversity* **2024**, *28*, 2135–2152.
- (17) Aldakheel, F. M.; Alduraywish, S. A.; Dabwan, K. H. *Scientific Reports* **2025**, *15*, 12764.
- (18) Zdrzil, B.; Felix, E.; Hunter, F.; Manners, E. J.; Blackshaw, J.; Corbett, S.; De Veij, M.; Ioannidis, H.; Lopez, D. M.; Mosquera, J. F., et al. *Nucleic acids research* **2024**, *52*, D1180–D1192.
- (19) Pedregosa, F.; Varoquaux, G.; Gramfort, A.; Michel, V.; Thirion, B.; Grisel, O.; Blondel, M.; Prettenhofer, P.; Weiss, R.; Dubourg, V., et al. *the Journal of machine Learning research* **2011**, *12*, 2825–2830.
- (20) Grisoni, F.; Consonni, V.; Todeschini, R. In *Computational chemogenomics*; Springer: 2018, pp 171–209.
- (21) Chithrananda, S.; Grand, G.; Ramsundar, B. *arXiv preprint arXiv:2010.09885* **2020**.
- (22) Li, M.; Zhou, J.; Hu, J.; Fan, W.; Zhang, Y.; Gu, Y.; Karypis, G. *ACS Omega* **2021**.
- (23) Veličković, P.; Cucurull, G.; Casanova, A.; Romero, A.; Liò, P.; Bengio, Y. Graph Attention Networks, 2018.
- (24) Kearnes, S.; McCloskey, K.; Berndl, M.; Pande, V.; Riley, P. *Journal of computer-aided molecular design* **2016**, *30*, 595–608.
- (25) Gilmer, J.; Schoenholz, S. S.; Riley, P. F.; Vinyals, O.; Dahl, G. E. Neural Message Passing for Quantum Chemistry, 2017.
- (26) Xiong, Z.; Wang, D.; Liu, X.; Zhong, F.; Wan, X.; Li, X.; Li, Z.; Luo, X.; Chen, K.; Jiang, H., et al. *Journal of medicinal chemistry* **2019**, *63*, 8749–8760.